THE JOURNAL OF NAVIGATION (2016), **69**, 561–581.
doi:10.1017/S0373463315000752

Improved Underwater Integrated Navigation System using Unscented Filtering Approach

Mohammad Shabani and Asghar Gholami

(*Electrical & Computer Engineering Dept., Isfahan University of Technology, Isfahan 84156-83111, Iran*)
(E-mail: m.shabanisheijani@ec.iut.ac.ir)

In underwater navigation, the conventional Error State Kalman Filter (ESKF) is used for combining navigation data where due to first order linearization of the nonlinear equations of the dynamics and measurements, considerable error is induced in estimated error state and covariance matrices. This paper presents an underwater integrated inertial navigation system using the unscented filter as an improved nonlinear version of the Kalman filter family. The designed system consists of a strap-down inertial navigation system accompanying Doppler velocity log and depth meter. In the proposed approach, to use the nonlinear capabilities of the unscented filtering approach the integrated navigation system is implemented in a direct approach where the nonlinear total state dynamic and and measurement models are utilised without any linearization. To our knowledge, no results have been reported in the literature on the experimental evaluation of the unscented-based integrated navigation system for underwater vehicles. The performance of the designed system is studied using real measurements. The results of the lake test show that the proposed system estimates the vehicle's position more accurately compared with the conventional ESKF structure.

KEYWORDS

1. Strap-down Inertial Navigation System. 2. Underwater Integrated Navigation System. 3. Error State Kalman Filter. 4. Unscented Filtering.

Submitted: 16 June 2014. Accepted: 20 September 2015. First published online: 30 October 2015.

1. INTRODUCTION. Underwater vehicles are used for a wide range of applications, including underwater mapping, oceanographic and bathymetric surveys and repair and inspection of subsea infrastructures in the oil and gas industries (Kinsey et al., 2006; Leonard et al., 1998). The traditional approach for navigation of underwater vehicles is dead reckoning (DR) (Brokloff, 1997; Kinsey and Whitcomb, 2007). In the two-dimensional DR approach, the current position is calculated knowing the previous position and measurements of the velocity and heading (Groves, 2008; Titterton and Weston, 2004; Hide et al., 2006). In underwater navigation, the velocity of the vehicle is measured using a Doppler Velocity Log (DVL) and the heading measurement is provided by a compass. Because the DVL needs at least

three beams to measure the bottom track velocity, it would malfunction under conditions of large roll and pitch. Furthermore, the DVL's ping rate is generally slow (3–7 Hz) and dependency of the DVL signal on the acoustic environment causes the DVL to occasionally be unavailable (Farrell, 2008). The other disadvantage of the DR approach arises from the inaccuracy of the velocity data caused by internal biasing errors, external random errors and also error in heading measurement which causes the position error to grow with time due to the error in transformation of the velocity from body frame to navigation frame and time integration of the velocity signal (Jalving et al., 2003).

A Strap-down Inertial Navigation System (SINS) estimates position, velocity, and orientation of the vehicle using the signals measured by an Inertial Measurement Unit (IMU) and is based on the dead-reckoning principle (Pitman, 1962; Britting, 1971; Moore et al., 2008). The IMU is composed of a triad of orthogonal accelerometers and gyroscopes. Due to different noise sources in accelerometers and gyroscopes, and the successive time integration of the acceleration, the position error increases with time (Jekeli, 2001; Grewal et al., 2007; Atia et al., 2014). In order to bound the error growth, the SINS is used together with other navigation aids. In an underwater integrated navigation system, it is common to use auxiliary sensors such as the DVL, compass, depth meter, Global Positioning System (GPS) and Acoustic Positioning System (APS) to reduce the position error. Systems with several beacons mounted on a surface vessel have largely been superseded by Ultra-Short Baseline (USBL) systems. These use a single-phase array transponder on the ship that enables direction to be measured as well as range (Kinsey et al., 2006; Stutters et al., 2008; Paull et al., 2014).

Over the last decade, numerous papers have utilised these sensors for underwater vehicle navigation (Yun et al., 1999; Larsen, 2000; McEwen et al., 2005; Kussat et al., 2005; Jo and Choi, 2006; Lee et al., 2007; Miller et al., 2010; Hegrenaes and Hallingstad, 2011; Shabani et al., 2015). Due to unavailability of GPS signals under the water, it is not possible to correct the SINS output using GPS data (Grenon et al., 2001; Marco and Healey, 2001). APS are alternative approaches for aiding the SINS in underwater applications. However, since these types of system utilise several beacons to be either installed on the sea floor or mounted to a surface vessel, their operation range is restricted. In addition, the calibration and alignment of the beacons are time consuming and installation and maintenance of such systems are expensive (Stutters et al., 2008; Grenon et al., 2001). In order to perform independent underwater navigation, the use of on board auxiliary sensors, such as depth meter, DVL and compass are indispensable. Such sensors may be used to correct the SINS output without the need to use sources outside the vehicle.

In the strap-down underwater integrated navigation system, the DVL plays a critical role in bounding the SINS drift. However, over time intervals where the DVL is unavailable, the position error of the SINS increases quickly with time. Thus, due to a nonlinear dynamic system, the type of prediction algorithm becomes increasingly important. The prevalent method for incorporating the SINS output and the auxiliary signals is the Kalman filter (Grewal and Andrews, 2008; Brown and Hwang, 1997; Bar-Shalom et al., 2001). In the last decade, in many cases, indirect filtering has been utilised for correcting the drift of the SINS output in underwater integrated navigation systems (Larsen, 2000; Jo and Choi, 2006; Lee et al., 2007; Miller et al., 2010; Hegrenaes and Hallingstad, 2011; Zhao and Gao, 2004).

In this structure, as shown in Figure 1, differences between SINS outputs and auxiliary measurements are used by the Error State Kalman Filter (ESKF) to estimate the errors of position, velocity and orientation. Finally, the SINS outputs are corrected by the estimated errors. In this structure, the corrected state is fed back into the SINS to update it (Maybeck, 1979; Farrell and Barth, 1999). Due to strong nonlinearity of the dynamic and measurement equations in the underwater integrated navigation system, linearization of these equations using the first order term of the Taylor series expansion leads to a substantial error in the estimates of error states and covariance matrix (Arasaratnam, 2009; Van der Merwe, 2004). Therefore, first order linearization in the ESKF causes the performance of the system to degrade, which can give rise to errors in the estimated position. In order to mitigate the errors caused by first order linearization employed by the ESKF, we are required to use a nonlinear filtering approach. To solve the linearization problem, the unscented filter was proposed to more accurately estimate the mean and covariance of the system's state (Julier and Uhmann, 1997; 2004). In the unscented filter, it is not required to linearize the nonlinear dynamic and measurement models through Jacobian derivations. Instead, by using the unscented transform, a set of deterministically selected sigma points is used which completely capture the true mean and covariance of the random vector. Then, these sigma points are propagated through the nonlinear functions. This algorithm captures the mean and covariance accurately to the three-order term of the Taylor series expansions for arbitrary nonlinear functions (Julier et al., 2000; Wan and Van der Merwe, 2000). Arasaratnam and Haykin (2009) proposed the Cubature Kalman Filter (CKF) where the third order spherical cubature integration rule was used for estimating the mean and covariance of the system's state. In their paper, they claimed that the cubature integration method is more accurate than the unscented filter. However, Sarkka (2013) showed that the CKF is a special case of the unscented filter by choosing the special values of the UKF's scaling parameters.

For more accurately estimating the mean and covariance matrix of the navigation system's state and also preventing divergence of the filter, we propose a strap-down integrated navigation system using an unscented-based filtering approach for underwater applications.

Research on the unscented-based underwater integrated navigation system is scarce. Foss and Meland (2007) implemented the unscented filter for combining measurements from different sensors for an underwater vehicle and utilised numerical simulations for testing it. Yoon et al. (2003) proposed a location estimation algorithm where the GPS and Inertial Navigation System (INS) signals were combined by the UKF. In another study (Benzerrouk et al., 2013), an adaptive cubature INS/GNSS integrated navigation system was presented for aerospace applications and evaluated in simulations. Gao et al. (2014) also proposed a SINS-BeiDou-DVL integrated navigation system based on a CKF for marine applications and its performance was examined through numerical simulations.

To the best of our knowledge, this paper presents the first experimental evaluation of an unscented filtering-based SINS for underwater vehicles. In the proposed algorithm, a nonlinear equation for the DVL measurement model is derived. Consequently, both the dynamic and the measurement equations for implementing the filter are nonlinear. In order to utilise the nonlinear capabilities of the unscented algorithm, the integration navigation system is implemented in a direct approach (Figure 2) (Maybeck, 1979; Farrell and Barth 1999), where the total states of the system are used instead of

https://doi.org/10.1017/S0373463315000752 Published online by Cambridge University Press

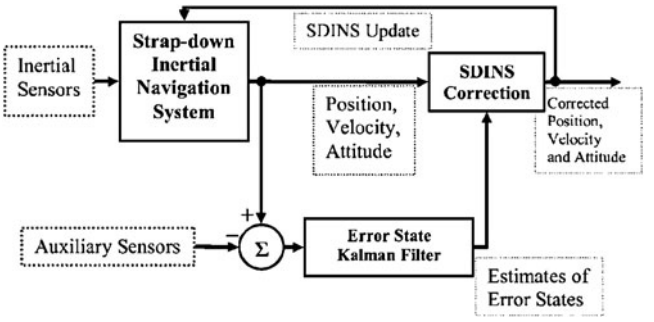

Figure 1. Indirect filtering.

error states. In this approach, unlike the indirect structure where the SINS and the prediction stage of the Kalman Filter (KF) are implemented into two distinct blocks, these two functions are merged and the correction stage of the filter operates asynchronously.

In addition, to exploit the unscented filter in the integrated navigation system, the roll and pitch signals computed from the accelerometer measurements are also used as auxiliary signals. Although, from a theoretical point of view, the processing of the same measurements in both prediction and correction stages is not completely correct, this technique works well in practice (Georgy et al., 2011). Since GPS is not available underwater and DVL also have dropouts, this technique can limit the drift in the roll and pitch signals estimated from the gyroscopes, which, in turn, is the main origin of the growth of the position error (Skog and Handel, 2009). The performance of the SINS/DVL integration system is investigated via a lake test in a surface vessel and compared with a similar system implemented by the ESKF. In Section 4, we show that the proposed algorithm estimates the output state more accurately than the prevalent ESKF structure.

The structure of this paper is as follows. After the Introduction, in Section 2, the equations related to the unscented filter are reviewed. In Section 3, the implemented system is described and related equations are derived. In Section 4, the performance of the designed system is evaluated using the results of the experimental tests. Finally, conclusions are presented in Section 5.

2. UNSCENTED INTEGRATION METHOD.

Due to nonlinearity of the dynamic equations of navigation, the general form of a continuous time non-linear state space model (Simon, 2006) may expressed as:

$$\dot{\mathbf{x}} = \mathbf{f}(\mathbf{x}, \mathbf{u}) + \mathbf{G}\mathbf{w}, \quad \mathbf{w} \sim \mathbf{N}(0, \mathbf{Q_c}) \tag{1}$$

Where $\mathbf{x}$ is the total state vector of the system which is given as follows:

$$\mathbf{x} = \begin{bmatrix} \mathbf{p}^n \\ \mathbf{v}^n \\ \Theta \\ \mathbf{b}_a \\ \mathbf{b}_g \end{bmatrix} \tag{2}$$

https://doi.org/10.1017/S0373463315000752 Published online by Cambridge University Press

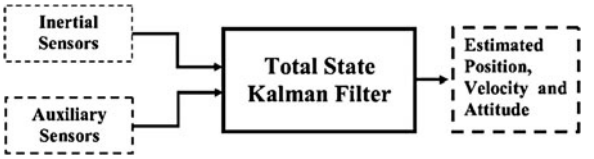

Figure 2. Direct filtering.

$\mathbf{p}^n = [L, l, Z]^T$ is the position vector of the vehicle in the navigation frame which includes the latitude, longitude, and the depth of the vehicle relative to the water surface. $\mathbf{v}^n = [v_N, v_E, v_D]^T$ is the velocity vector resolved in the navigation frame which is included in the north velocity, east velocity, and down velocity. $\Theta = [\varphi, \theta, \psi]^T$ is the orientation vector of the body frame with respect to navigation frame (North, East, and Down directions). $\mathbf{b}_a = [b_{ax}, b_{ay}, b_{az}]^T$ is the vector of the accelerometer bias and $\mathbf{b}_g = [b_{gx}, b_{gy}, b_{gz}]^T$ is the vector of the gyroscope bias. The inertial sensors' biases are modelled as a random walk plus a random constant (Maybeck, 1979; Farrell, 2008):

$$\dot{\mathbf{b}}_a = \boldsymbol{\eta}_a, \quad \boldsymbol{\eta}_a \sim \mathrm{N}\left(\mathbf{0}, \sigma_{b_a}^2 \mathbf{I}\right) \tag{3}$$

$$\dot{\mathbf{b}}_g = \boldsymbol{\eta}_g, \quad \boldsymbol{\eta}_g \sim \mathrm{N}\left(\mathbf{0}, \sigma_{b_g}^2 \mathbf{I}\right) \tag{4}$$

Where $\boldsymbol{\eta}_a$ and $\boldsymbol{\eta}_g$ are Gaussian white noise vectors with variances $\sigma_{b_a}^2 \mathbf{I}$ and $\sigma_{b_g}^2 \mathbf{I}$, respectively. Throughout, the symbol N represents the normal distribution and $\mathbf{I}$ is the identity matrix.

$\mathbf{f}$ is the system nonlinear function which describes the dynamic behaviour of the system. $\mathbf{G}$ is the dynamic noise distribution. The control input $\mathbf{u}$ is given by:

$$\mathbf{u} = \begin{bmatrix} \mathbf{f}^b \\ \boldsymbol{\omega}_{ib}^b \end{bmatrix} \tag{5}$$

Where $\mathbf{f}^b = [f_x, f_y, f_z]^T$ and $\boldsymbol{\omega}_{ib}^b = [p, q, r]^T$ are the specific force and angular rate of the IMU relative to inertial frame, resolved in the IMU frame respectively, measured by the inertial sensors (Farrell, 2008; Groves, 2008). $\mathbf{w}$, in Equation (1), is the process noise due to uncertainty in the control inputs and is modelled in the KF as a Gaussian white noise vector with zero mean and a Power Spectral Density (PSD) $\mathbf{Q}_c$, which may be expressed as follows:

$$\mathbf{w} = \begin{bmatrix} \mathbf{w}_a \\ \mathbf{w}_g \\ \boldsymbol{\eta}_a \\ \boldsymbol{\eta}_g \end{bmatrix} \tag{6}$$

Where $\mathbf{w}_a = [w_{ax}, w_{ay}, w_{az}]^T$ and $\mathbf{w}_g = [w_{gx}, w_{gy}, w_{gz}]^T$ are random noise components of the accelerometers and gyroscopes in x, y and z directions of the IMU axes,

https://doi.org/10.1017/S0373463315000752 Published online by Cambridge University Press

respectively and $\mathbf{Q}_c$ is a diagonal matrix as follows:

$$\mathbf{Q}_c = \begin{pmatrix} \zeta_a^2\mathbf{I}_3 & \mathbf{0}_3 & \mathbf{0}_3 & \mathbf{0}_3 \\ \mathbf{0}_3 & \zeta_g^2\mathbf{I}_3 & \mathbf{0}_3 & \mathbf{0}_3 \\ \mathbf{0}_3 & \mathbf{0}_3 & \zeta_{b_a}^2\mathbf{I}_3 & \mathbf{0}_3 \\ \mathbf{0}_3 & \mathbf{0}_3 & \mathbf{0}_3 & \zeta_{b_g}^2\mathbf{I}_3 \end{pmatrix} \tag{7}$$

Where ζ_a, ζ_g, ζ_{b_a} and ζ_{b_g} are the root power spectral density of the accelerometers' noise, gyroscopes' noise, accelerometers' bias and gyroscopes' bias, respectively. $\mathbf{I}_3$ and $\mathbf{0}_3$ are the 3×3 unit and zero matrices, respectively. Assuming that the noise characteristics of all accelerometers and all gyroscopes in x, y and z directions of the IMU axes are equal (Groves, 2008; Niu et al., 2007):

$$\zeta_a = \sigma_a\sqrt{dt},\ \zeta_g = \sigma_g\sqrt{dt} \tag{8}$$

$$\zeta_{b_a} = \sigma_{b_a}\sqrt{\tau_{b_a}},\ \zeta_{b_g} = \sigma_{b_g}\sqrt{\tau_{b_g}} \tag{9}$$

Where σ_a is the standard deviation of the accelerometer's noise, σ_g is the standard deviation of the gyroscope's noise, dt is the sampling time of inertial sensors, σ_{b_a} and σ_{b_g} are the standard deviations of the accelerometer and gyroscope bias, respectively and τ_{b_a} and τ_{b_g} are their correlation time. In this paper, the specifications of the inertial sensors provided by manufacturers are used to determine the system noise PSDs (Groves, 2008).

In the proposed approach, the auxiliary measurements of the system are a nonlinear combination of the states which are corrupted with noise. This can be given in terms of the total states of the system by the following equation:

$$\mathbf{y} = \mathbf{h}(\mathbf{x}) + \boldsymbol{\nu}, \quad \boldsymbol{\nu} \sim \mathrm{N}(\mathbf{0}, \mathbf{R}) \tag{10}$$

Where $\mathbf{y}$ is the measurement vector of the system that is defined as follows:

$$\mathbf{y} = \begin{bmatrix} Z_m \\ \mathbf{v}_m^b \\ \Theta_m \end{bmatrix} \tag{11}$$

Where Z_m is the auxiliary signal of depth, $\mathbf{v}_m^b = [v_x,\ v_y,\ v_z]^T$ are the measurements of the DVL in the body frame, and $\Theta_m = [\varphi_m,\ \theta_m,\ \psi_m]^T$ are the auxiliary signals of orientation. The roll and pitch measurements are computed by the accelerometer signals and heading measurement is provided by a compass.

$\mathbf{h}$, in Equation (6), is the measurement model function and $\boldsymbol{\nu}$ represents the measurement noise which is assumed to be a zero mean, Gaussian white-noise process with known covariance matrix $\mathbf{R}$.

The discrete-time form of the Equations (1) may be expressed by:

$$\mathbf{x}_k = \mathbf{f}(\mathbf{x}_{k-1},\ \mathbf{u}_{k-1}) + \mathbf{q}_{k-1}, \quad \mathbf{q}_{k-1} \sim \mathrm{N}(\mathbf{0},\ \mathbf{Q}_{k-1}) \tag{12}$$

Where $\mathbf{x}_k$ and $\mathbf{u}_k$ are the total state vector of the system and the control input at discrete time k, respectively. $\mathbf{q}_k$ is the process noise with covariance matrix $\mathbf{Q}_k$ at time step k (Jekeli, 2001; Farrell, 2008):

$$\mathbf{Q}_{k-1} \approx \mathbf{G}_{k-1}\mathbf{Q}_c\, dt\mathbf{G}_{k-1}^T \tag{13}$$

https://doi.org/10.1017/S0373463315000752 Published online by Cambridge University Press

The discrete-time form of the Equations (10) may be given by the following equation:

$$\mathbf{y}_k = \mathbf{h}(\mathbf{x}_k) + \mathbf{r}_k, \quad \mathbf{r}_k \sim \mathrm{N}(\mathbf{0}, \mathbf{R}_k) \tag{14}$$

Where $\mathbf{y}_k$ is the measurement vector of the system at discrete time k. $\mathbf{r}_k$ is the measurement noise vector with covariance matrix $\mathbf{R}_k$ at time step k. In many navigation applications, due to being independent, the individual components of the measurement noise vector, $\mathbf{R}_k$ are considered as a diagonal matrix (Groves, 2008; Grewal and Andrews, 2008).

The unscented filter can be derived as an approximation of the general Gaussian filter. In order to construct the Gaussian filter, the moment matching approximations are used and also the filtering distribution is assumed as Gaussian (Arasaratnam, 2009; Sarkka, 2013).

$$p(\mathbf{x}_k|\mathbf{y}_k) \cong \mathrm{N}(\mathbf{x}_k|\hat{\mathbf{x}}_k, \mathbf{P}_k) \tag{15}$$

Where $\hat{\mathbf{x}}_k$ and $\mathbf{P}_k$ are the mean and the covariance of the Gaussian distribution, respectively.

The prediction stage of the Gaussian filter with additive noise is given as follows:

$$\begin{aligned} \hat{\mathbf{x}}_k^- &= \mathrm{E}[\mathbf{x}_k|\mathbf{y}_{1:k-1}] \\ &= \mathrm{E}[\mathbf{f}(\mathbf{x}_{k-1}, \mathbf{u}_{k-1}) + \mathbf{q}_{k-1}|\mathbf{y}_{1:k-1}] \end{aligned} \tag{16}$$

Since $\mathbf{q}_{k-1}$ is zero-mean Gaussian, we get

$$\begin{aligned} \hat{\mathbf{x}}_k^- &= \mathrm{E}[\mathbf{f}(\mathbf{x}_{k-1}, \mathbf{u}_{k-1})|\mathbf{y}_{1:k-1}] \\ &= \int \mathbf{f}(\mathbf{x}_{k-1}, \mathbf{u}_{k-1}) p(\mathbf{x}_{k-1}|\mathbf{y}_{1:k-1}) d\mathbf{x}_{k-1} \\ &= \int \mathbf{f}(\mathbf{x}_{k-1}, \mathbf{u}_{k-1}) \mathrm{N}\left(\mathbf{x}_{k-1}|\hat{\mathbf{x}}_{k-1}^+, \hat{\mathbf{P}}_{k-1}^+\right) d\mathbf{x}_{k-1} \end{aligned} \tag{17}$$

$$\begin{aligned} \mathbf{P}_k^- &= \mathrm{E}\left[\left(\mathbf{x}_k - \hat{\mathbf{x}}_k^-\right)\left(\mathbf{x}_k - \hat{\mathbf{x}}_k^-\right)^T \middle| \mathbf{y}_{1:k-1}\right] \\ &= \int \left(\mathbf{f}(\mathbf{x}_{k-1}, \mathbf{u}_{k-1}) - \hat{\mathbf{x}}_k^-\right)\left(\mathbf{f}(\mathbf{x}_{k-1}, \mathbf{u}_{k-1}) - \hat{\mathbf{x}}_k^-\right)^T \mathrm{N}\left(\mathbf{x}_{k-1}|\hat{\mathbf{x}}_{k-1}^+, \hat{\mathbf{P}}_{k-1}^+\right) d\mathbf{x}_{k-1} + \mathbf{Q}_{k-1} \end{aligned} \tag{18}$$

Where E is the expectation operator, $\hat{\mathbf{x}}_k^-$ and $\mathbf{P}_k^-$ are the predicted mean and covariance of the Gaussian filter at the time step k.

Similarly to the prediction stage, the correction stage of the Gaussian filter is expressed by:

$$\hat{\mathbf{z}}_k = \int \mathbf{h}(\mathbf{x}_k) \mathrm{N}\left(\mathbf{x}_k|\hat{\mathbf{x}}_k^-, \hat{\mathbf{P}}_k^-\right) d\mathbf{x}_k \tag{19}$$

$$\mathbf{P}_{yy,\,k} = \int \left(\mathbf{h}(\mathbf{x}_k) - \hat{\mathbf{z}}_k\right)\left(\mathbf{h}(\mathbf{x}_k) - \hat{\mathbf{z}}_k\right)^T \mathrm{N}\left(\mathbf{x}_k|\hat{\mathbf{x}}_k^-, \hat{\mathbf{P}}_k^-\right) d\mathbf{x}_k + \mathbf{R}_k \tag{20}$$

$$\mathbf{P}_{xy,\,k} = \int \left(\mathbf{x}_k - \hat{\mathbf{x}}_k^-\right)\left(\mathbf{h}(\mathbf{x}_k) - \hat{\mathbf{z}}_k\right)^T \mathrm{N}\left(\mathbf{x}_k|\hat{\mathbf{x}}_k^-, \hat{\mathbf{P}}_k^-\right) d\mathbf{x}_k \tag{21}$$

$$\mathbf{K}_k = \mathbf{P}_{xy,\,k} \mathbf{P}_{yy,\,k}^{-1} \tag{22}$$

$$\hat{\mathbf{x}}_k^+ = \hat{\mathbf{x}}_k^- + \mathbf{K}_k(\mathbf{y}_k - \hat{\mathbf{z}}_\mathbf{k}) \tag{23}$$

$$\mathbf{P}_k^+ = \mathbf{P}_k^- + \mathbf{K}_k \mathbf{P}_{yy,\,k} \mathbf{K}_k^T \tag{24}$$

https://doi.org/10.1017/S0373463315000752 Published online by Cambridge University Press

Where $\hat{\mathbf{z}}_k$ is the predicted measurement, $\mathbf{P}_{yy,k}$ is the innovation covariance, $\mathbf{P}_{xy,k}$ is the cross-covariance matrix, $\mathbf{K}_k$ is the filter gain matrix and $\hat{\mathbf{x}}_k^+$ and $\mathbf{P}_k^+$ are the corrected mean and covariance of the Gaussian filter at the time step k, respectively.

The moment matching formulation makes possible the utilisation of the numerical approaches like the cubature integration methods for computing the multi-dimensional integrals of the form $\int \mathbf{g}(\mathbf{x})\mathrm{N}(\mathbf{x}|\hat{\mathbf{x}}, \mathbf{P})d\mathbf{x}$, where $\mathbf{g}(\mathbf{x})$ is an arbitrary non-linear function.

It can be shown that the computation of the aforementioned integral may be accomplished using the third order spherical cubature rule as follows (Arasaratnam, 2009; Sarkka, 2013):

- Calculate the $2n$ cubature or sigma points by:

$$\chi^{(i)} = \begin{cases} \sqrt{n}\mathbf{e}_i, & i = 1, \ldots, n \\ -\sqrt{n}\mathbf{e}_{i-n}, & i = n+1, \ldots, 2n \end{cases} \tag{25}$$

  Where n is the dimension of the state vector and $\mathbf{e}_i$ is an n-component unit vector in the direction of coordinate axis i. In general, $\chi^{(i)}$ is generated as follows:

$$\chi^{(i)} = \left\{ \begin{pmatrix} \sqrt{n} \\ 0 \\ 0 \\ \vdots \\ 0 \end{pmatrix}, \begin{pmatrix} 0 \\ \sqrt{n} \\ 0 \\ \vdots \\ 0 \end{pmatrix}, \ldots, \begin{pmatrix} 0 \\ 0 \\ 0 \\ \vdots \\ \sqrt{n} \end{pmatrix}, \begin{pmatrix} -\sqrt{n} \\ 0 \\ 0 \\ \vdots \\ 0 \end{pmatrix}, \begin{pmatrix} 0 \\ -\sqrt{n} \\ 0 \\ \vdots \\ 0 \end{pmatrix}, \ldots, \begin{pmatrix} 0 \\ 0 \\ 0 \\ \vdots \\ -\sqrt{n} \end{pmatrix} \right\} \tag{26}$$

- Compute the integral by:

$$\int \mathbf{g}(\mathbf{x})\mathrm{N}(\mathbf{x}|\hat{\mathbf{x}}, \mathbf{P})d\mathbf{x} \approx \frac{1}{2n}\sum_{i=1}^{2n} \mathbf{g}\left(\hat{\mathbf{x}} + \sqrt{\mathbf{P}}\chi^{(i)}\right) \tag{27}$$

Where the square root of the matrix $\mathbf{P}(\sqrt{\mathbf{P}} = \mathbf{C})$ can be calculated by solving the Cholesky decomposition equation $\mathbf{P} = \mathbf{C}\mathbf{C}^T$ for a symmetric, nonnegative definite matrix (Grewal and Andrews, 2008).

3. INTEGRATED NAVIGATION SYSTEM EQUATIONS.

In this section, the system and measurement equations for the total states of navigation are derived and the procedure of the designed system is described.

3.1. *The system equations.*

The system nonlinear functions $\mathbf{f}$ described in Equation (1) are given as follows (Farrell, 2008; Britting, 1971):

$$\dot{\mathbf{p}}^n = \mathrm{Y}\mathbf{v}^n \tag{28}$$

$$\dot{\mathbf{v}}^n = \mathbf{C}_b^n\left(\mathbf{f}^b - \mathbf{b}_a\right) - \left(2\boldsymbol{\omega}_{ie}^n + \boldsymbol{\omega}_{en}^n\right) \times \mathbf{v}^n + \mathbf{g}^n \tag{29}$$

$$\dot{\Theta} = \Lambda^{-1}\boldsymbol{\omega}_{nb}^b \tag{30}$$

$$\dot{\mathbf{b}}_a = 0 \tag{31}$$

$$\dot{\mathbf{b}}_g = 0 \tag{32}$$

https://doi.org/10.1017/S0373463315000752 Published online by Cambridge University Press

Where

$$\mathrm{Y} = \begin{pmatrix} \dfrac{1}{R_N - Z} & 0 & 0 \\ 0 & \dfrac{\sec L}{R_E - Z} & 0 \\ 0 & 0 & 1 \end{pmatrix} \tag{33}$$

$$\mathbf{f}^b = \left[f_x, f_y, f_z\right]^T \tag{34}$$

$$\boldsymbol{\omega}_{ie}^n = \left[\Omega \cos L,\ 0,\ -\Omega \sin L\right]^T \tag{35}$$

$$\boldsymbol{\omega}_{en}^n = \left[\frac{v_E}{R_E - Z},\ \frac{v_N}{R_N - Z},\ -\frac{v_E \tan L}{R_E - Z}\right]^T \tag{36}$$

$$\mathbf{g}^n = \left[0,\ 0,\ g\right]^T \tag{37}$$

$$\Lambda = \begin{pmatrix} 1 & 0 & -\sin\theta \\ 0 & \cos\phi & \sin\phi\cos\theta \\ 0 & -\sin\phi & \cos\phi\cos\theta \end{pmatrix} \tag{38}$$

$$\boldsymbol{\omega}_{nb}^b = \left[\omega_x,\ \omega_y,\ \omega_z\right]^T = \left(\boldsymbol{\omega}_{ib}^b - \mathbf{b}_g\right) - \mathbf{C}_b^n\left[\boldsymbol{\omega}_{ie}^n + \boldsymbol{\omega}_{en}^n\right] \tag{39}$$

$$R_N = \frac{R\left(1 - e^2\right)}{\left(1 - e^2 \sin^2(L)\right)^{1{\cdot}5}} \tag{40}$$

$$R_E = \frac{R}{\left(1 - e^2 \sin^2(L)\right)^{0{\cdot}5}} \tag{41}$$

The variables R_N, R_E, R, e and Ω represent the meridian radius of curvature, the transverse radius of curvature, the length of the semi-major axis, the major eccentricity of the ellipsoid of the Earth, and the Earth's angular rate, respectively (Titterton and Weston, 2004). $\mathbf{C}_b^n$ is the transformation matrix from body to navigation axes which may be expressed by the following equation:

$$\mathbf{C}_b^n = \begin{pmatrix} \cos\theta\cos\psi & -\cos\varphi\sin\psi + \sin\varphi\sin\theta\cos\psi & \sin\varphi\sin\psi + \cos\varphi\sin\theta\cos\psi \\ \cos\theta\sin\psi & \cos\varphi\cos\psi + \sin\varphi\sin\theta\sin\psi & -\sin\varphi\cos\psi + \cos\varphi\sin\theta\sin\psi \\ -\sin\theta & \sin\varphi\cos\theta & \cos\varphi\sin\theta \end{pmatrix} \tag{42}$$

$\mathbf{f}^b$ represents the specific force in body axes. $\boldsymbol{\omega}_{ie}^n$ is the angular rate of the Earth expressed in the navigation frame. $\boldsymbol{\omega}_{en}^n$ represents the angular rate of the navigation frame with respect to the Earth-fixed frame. $\mathbf{g}^n$ and g are the gravity vector in the navigation frame and the Earth gravity constant, respectively. $\boldsymbol{\omega}_{nb}^b$ is the angular rate of the vehicle with respect to the navigation frame. $\boldsymbol{\omega}_{ib}^b = [p,\ q,\ r]^T$ is the angular rate of the vehicle. The gravity g is computed by the following equation (Titterton and Weston, 2004):

$$g = \frac{g_0}{1 - Z/R_0} \tag{43}$$

https://doi.org/10.1017/S0373463315000752 Published online by Cambridge University Press

Where

$$g_0 = 9{\cdot}780318 \times \left(1 + 5{\cdot}3024 \times 10^{-3} \sin^2 L - 5{\cdot}9 \times 10^{-6} \sin^2 2L\right) \tag{44}$$

$$R_0 = \sqrt{R_N R_E} \tag{45}$$

3.2. *The measurement equations.* In this section, the measurement equations used in this paper, including the depth, velocity, roll, pitch, and heading are derived.

The measurement equation of the depth meter and its measurement noise variance are defined by:

$$Z_m = Z + \nu_z \tag{46}$$

$$R_z = \sigma_z^2 \tag{47}$$

Where ν_z and σ_z^2 is the measurement noise and the measurement noise variance of the depth meter, respectively.

The relationship between the DVL's measurements and the states of the velocity may be expressed by the following nonlinear equation:

$$\mathbf{v}_m^b = \mathbf{C}_n^b \mathbf{v}^n + \boldsymbol{\nu}_v \tag{48}$$

This equation can be expressed in component form as follows:

$$v_x = C_{11} v_N + C_{21} v_E + C_{31} v_D + \nu_{v_x} \tag{49}$$

$$v_y = C_{12} v_N + C_{22} v_E + C_{32} v_D + \nu_{v_y} \tag{50}$$

$$v_z = C_{13} v_N + C_{23} v_E + C_{33} v_D + \nu_{v_z} \tag{51}$$

Where C_{ij} is the element in the ith row and the jth column of the transformation matrix from body frame to navigation frame (i.e. $\mathbf{C}_n^b$), $[v_N, v_E, v_D]$ is the north, east and down velocity components and $\nu_v = \left[\nu_{v_x}, \nu_{v_y}, \nu_{v_z}\right]$ is the measurement noise vector of the DVL.

It can be shown that the covariance matrix of the DVL measurements caused by instrumental noise is given by (Gilcoto et al., 2009):

$$\mathbf{R}_{dvl} = \begin{pmatrix} \dfrac{\sigma_{b_1}^2 + \sigma_{b_2}^2}{4\sin^2\beta} & 0 & \dfrac{\sigma_{b_1}^2 - \sigma_{b_2}^2}{8\sin\beta\cos\beta} \\ 0 & \dfrac{\sigma_{b_3}^2 + \sigma_{b_4}^2}{4\sin^2\beta} & \dfrac{\sigma_{b_4}^2 - \sigma_{b_3}^2}{8\sin\beta\cos\beta} \\ \dfrac{\sigma_{b_1}^2 - \sigma_{b_2}^2}{8\sin\beta\cos\beta} & \dfrac{\sigma_{b_4}^2 - \sigma_{b_3}^2}{8\sin\beta\cos\beta} & \dfrac{\sigma_{b_1}^2 + \sigma_{b_2}^2 + \sigma_{b_3}^2 + \sigma_{b_4}^2}{16\cos^2\beta} \end{pmatrix} \tag{52}$$

Where $\sigma_{b_i}^2$ is the variance of the radial velocity along the beam i (i = 1,2,3,4). It may be assumed that the radial velocity variances are equal which yields:

$$if\ \sigma_{b_1}^2 = \sigma_{b_2}^2 = \sigma_{b_3}^2 = \sigma_{b_4}^2 \Rightarrow \mathbf{R}_{dvl} = \begin{pmatrix} \sigma_{v_x}^2 & 0 & 0 \\ 0 & \sigma_{v_y}^2 & 0 \\ 0 & 0 & \sigma_{v_z}^2 \end{pmatrix} \tag{53}$$

Where $\sigma_{v_x}^2$, $\sigma_{v_y}^2$, and $\sigma_{v_z}^2$ are the variance of the DVL's measurements along its body frame.

https://doi.org/10.1017/S0373463315000752 Published online by Cambridge University Press

The measurement model of the roll and pitch may be given by:

$$\begin{aligned} \phi_m &= \phi + \nu_\phi \\ \theta_m &= \theta + \nu_\theta \end{aligned} \tag{54}$$

Where φ_m and θ_m are the auxiliary signals of the roll and pitch computed from the accelerometer's signals. Under circumstances where the vehicle is stationary or moves at a constant velocity (or cruising conditions), the only acceleration acting on the vehicle is the acceleration due to gravity (Grenon et al., 2001; Groves, 2008; Farrell, 2008). Therefore, the roll and pitch signals may be computed by the following equations:

$$\theta_m = \frac{\sin^{-1}(f_x)}{g} \tag{55}$$

$$\varphi_m = \frac{\sin^{-1}(f_y)}{g\cos(\theta_m)} \tag{56}$$

Where f_x and f_y are the accelerations acting on the vehicle along the forward and starboard directions measured by the accelerometers. When the following logical condition is true, the roll and pitch measurements are used in the correction stage of the integration filter (Farrell, 2008):

$$\left(\|\mathbf{f}^b\| - g < T_f\right) \text{and} \left(\|\boldsymbol{\omega}_{ib}^b\| < T_\omega\right) \tag{57}$$

Where T_f and T_ω are determined by trial and error. The symbol $\|\cdot\|$ denotes the norm of a vector.

Although, in theory, the roll and pitch signals are correlated to each other, as stated in Equation (56), one can assume that these signals are independent for small pitch angles:

$$\text{for small pitch angles} \Rightarrow \cos(\theta_m) \approx 1 \Rightarrow \begin{cases} \theta_m = \dfrac{\sin^{-1}(f_x)}{g} \\ \phi_m \approx \dfrac{\sin^{-1}(f_y)}{g} \end{cases} \tag{58}$$

This type of manoeuvre is performed in many marine applications, including the test conducted for this paper. Therefore, the measurement noise matrix for the signals of the roll and pitch is assumed to be diagonal as follows:

$$\mathbf{R}_\Theta = \begin{pmatrix} \sigma_\varphi^2 & 0 \\ 0 & \sigma_\theta^2 \end{pmatrix} \tag{59}$$

Where σ_φ^2 and σ_θ^2 are the variance of the signals of the roll and pitch, respectively. These quantities are calculated in terms of the variance of the acceleration signals according to Equation (58).

https://doi.org/10.1017/S0373463315000752 Published online by Cambridge University Press

The measurement equation of the compass and its measurement noise variance are defined by:

$$\psi_m = \psi + \nu_\psi \tag{60}$$

$$R_\psi = \sigma_\psi^2 \tag{61}$$

Where σ_ψ^2 is the variance of the compass measurement.

3.3. *Data integration.*

3.3.1. *The prediction stage.* In the prediction stage of the unscented filter, for each time step of inertial sensors, the total state of the system $\hat{\mathbf{x}}^-$ and covariance of the state $\mathbf{P}^-$ are predicted using Equations (12) and (13) and the unscented based integration method given by Equations (20)–(22).

In order to execute the prediction stage, the system equations can be expressed in component form as follows:

$$\dot{L} = \frac{v_N}{R_N + Z} \tag{62}$$

$$\dot{l} = \frac{v_E \sec(L)}{R_E + Z} \tag{63}$$

$$\dot{Z} = v_D \tag{64}$$

$$\dot{v}_N = f_N - v_E\left(2\Omega + \dot{l}\right)\sin(L) + v_D\dot{L} \tag{65}$$

$$\dot{v}_E = f_E - \left(2\Omega + \dot{l}\right)(v_N \sin(L) + v_D \cos(L)) \tag{66}$$

$$\dot{v}_D = f_D - v_E\left(2\Omega + \dot{l}\right)\cos(L) + v_N\dot{L} + g \tag{67}$$

$$\dot{\phi} = \left(\omega_y \sin\phi + \omega_x \cos\phi\right)\tan\theta + \omega_x \tag{68}$$

$$\dot{\theta} = \left(\omega_y \cos\phi - \omega_z \sin\phi\right) \tag{69}$$

$$\dot{\psi} = \left(\omega_y \sin\phi + \omega_z \cos\phi\right)\sec\theta \tag{70}$$

Where

$$f_N = C_{11}(f_x) + C_{12}(f_y) + C_{13}(f_z) \tag{71}$$

$$f_E = C_{21}(f_x) + C_{22}(f_y) + C_{23}(f_z) \tag{72}$$

$$f_D = C_{31}(f_x) + C_{32}(f_y) + C_{33}(f_z) \tag{73}$$

$$\omega_x = (p) + (C_{11}\omega_N + C_{21}\omega_E + C_{31}\omega_D) \tag{74}$$

$$\omega_y = (q) + (C_{12}\omega_N + C_{22}\omega_E + C_{32}\omega_D) \tag{75}$$

$$\omega_z = (r) + (C_{13}\omega_N + C_{23}\omega_E + C_{33}\omega_D) \tag{76}$$

And

$$\omega_N = \Omega\cos L + \frac{v_E}{R_E - Z} \tag{77}$$

$$\omega_E = -\frac{v_D}{R_N - Z} \tag{78}$$

$$\omega_D = -\Omega\sin L - \frac{v_E \tan L}{R_E - Z} \tag{79}$$

https://doi.org/10.1017/S0373463315000752 Published online by Cambridge University Press

Where C_{ij} is the element in the ith row and the jth column of the transformation matrix that is given by Equation (35).

3.3.2. *The correction stage.* Since auxiliary sensors are asynchronous or sampled at different rates, the correction stage is also executed asynchronously. Operating in asynchronous mode means that when measurements from one or more of the auxiliary sensors are received at time step k, the measurement parameters associated with those sensors ($\mathbf{y}_k$ and $\mathbf{R}_k$) are formed, and then the correction equations of the unscented filter are executed. In the event that none of the auxiliary sensors are available, the correction stage will not be executed. In this case, the filter continues to operate without correction using the prediction stage. The total state of the navigation and its covariance matrix are predicted with sampling frequency of inertial sensors according to Equations (12) and (13) with or without the correction stage.

On receiving of a new auxiliary signal $\mathbf{y}_k$, the navigation state $\hat{\mathbf{x}}^+$ and its associated covariance matrix $\mathbf{P}^+$ at time step k are corrected using Equations (14)–(19) and the unscented-based integration method expressed by Equations (20)–(22).

In the best case, where all of the auxiliary sensors are available, the measurement vector $\mathbf{y}$ and the matrix $\mathbf{R}$ are given as follows:

$$\mathbf{y} = \left[Z_m,\ v_x,\ v_y,\ v_z,\ \phi_m,\ \theta_m,\ \psi_m\right]^T \tag{80}$$

$$\mathbf{R} = \begin{bmatrix} \sigma_z^2 & 0 & 0 & 0 & 0 & 0 & 0 \\ 0 & \sigma_{v_x}^2 & 0 & 0 & 0 & 0 & 0 \\ 0 & 0 & \sigma_{v_y}^2 & 0 & 0 & 0 & 0 \\ 0 & 0 & 0 & \sigma_{v_z}^2 & 0 & 0 & 0 \\ 0 & 0 & 0 & 0 & \sigma_\phi^2 & 0 & 0 \\ 0 & 0 & 0 & 0 & 0 & \sigma_\theta^2 & 0 \\ 0 & 0 & 0 & 0 & 0 & 0 & \sigma_\psi^2 \end{bmatrix} \tag{81}$$

The dimensions of the correction parameters are determined based on the number of received auxiliary sensors. When one of the sensors is not received, the matrices associated with that sensor, which was given in Section 3.2, are removed from the correction parameters. The measurement noise matrix, $\mathbf{R}$, is determined by stationary measurements of the auxiliary sensors. However, due to external factors such as environmental vibration, the effective noise levels may be changed. Therefore, in order to obtain the optimal estimates, it is required to tune R (Groves, 2008). The flowchart of the unscented based integrated navigation system is illustrated in Figure 3.

4. EXPERIMENTAL RESULTS. In order to evaluate the performance of the proposed system, a lake test was accomplished. An instrumented vessel was utilised for the experiments as shown in Figure 4. The instruments used in the test include a fibre optic gyro IMU assembled by Sepahan Electronic Inc. with model Sarmad2, a DVL made by Jay Technology Inc., model IR/BQN_01 and a GPS receiver (NovAtelOEMV-1) installed on the vessel according to Figure 5. The GPS receiver is a single-frequency GPS receiver and its measurements were used only for position initialisation and reference purposes.

To evaluate the proposed approach, the inertial signals are incorporated with measurements of the DVL, depth meter, roll and pitch angles. The position estimated by

https://doi.org/10.1017/S0373463315000752 Published online by Cambridge University Press

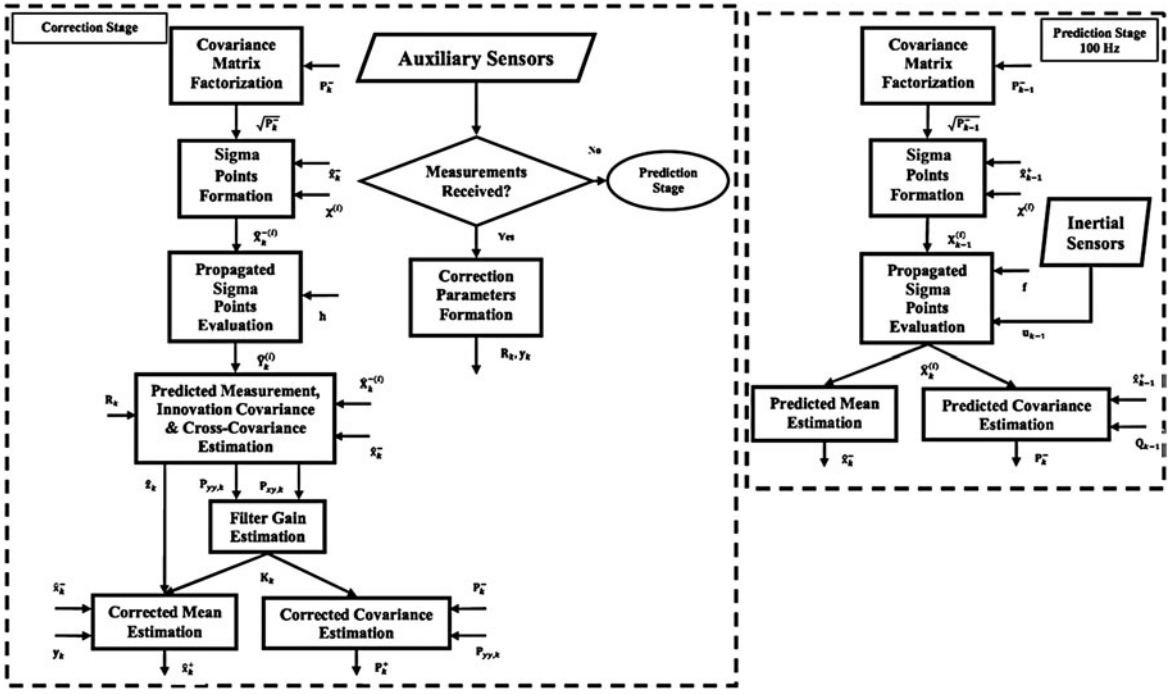

Figure 3. Strap-down integrated navigation system based on unscented based integration method.

https://doi.org/10.1017/S0373463315000752 Published online by Cambridge University Press

Figure 4. Instrumented vessel for experiments.

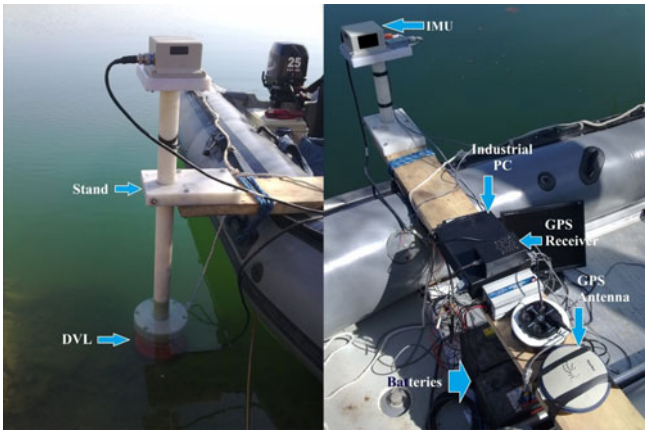

Figure 5. Instruments mounted on the vessel.

the proposed approach is compared with a position reference. In order to have an accurate position reference, two similar GPS receivers were used as a simple differential GPS. The first GPS receiver was installed at the origin point and the second one on the vessel and the position reference was calculated by subtracting smoothed data of the two GPS receivers. Our measurements showed that the accuracy of the calculated position reference was lower than 2 metres. As shown in Figure 5, a stand was used for holding the DVL under the water. The specifications of the instruments used can be found in Table 1 (Novatel, 2010).

In this paper, a trajectory composed of both the pseudo-sinusoid manoeuvres and the approximately straight track is used to show the performance of the designed system. The signals measured by the instruments are logged by a computer carried by the vessel and then post-processing of the collected data is carried out in the laboratory. To verify the accuracy of the proposed system, its estimated position is compared

https://doi.org/10.1017/S0373463315000752 Published online by Cambridge University Press

Table 1. Instrument specifications.

Gyroscope	
Bias Offset	±20°/hr
Bias Stability	1°/hr @ 1σ
Angular Random Walk	0·0667 °/$\sqrt{}$hr @ 1σ
Bandwidth	50 Hz
Data rate	100 Hz
Accelerometer	
Bias Offset	±50 mg
In Run Bias Variation	0·25 mg @ 1σ
Output Noise	55 µg/$\sqrt{}$Hz @ 1σ
Bandwidth	50 Hz
Data rate	100 Hz
DVL	
Frequency	300 kHz
Accuracy	1% ±2 mm/s @ 1σ
Maximum Altitude	300 m
Minimum Altitude	0·6 m
Maximum Velocity	±20 knots
Maximum Ping Rate	3 / second knots
GPS	
Position Reference Accuracy	<2 m (RMS)
Data Rate	5 Hz

with that of the ESKF-based integrated navigation system (Lee et al., 2007; Miller et al., 2010; Shabani et al., 2013).

According to Equations (8) and (9) and parameters given in Table 1, the matrix $\mathbf{Q}_c$ is considered as follows:

$$\mathbf{Q}_c = \begin{pmatrix} (9{\cdot}8\times10^{-5})^2\mathbf{I}_3 & \mathbf{0}_3 & \mathbf{0}_3 & \mathbf{0}_3 \\ \mathbf{0}_3 & (2{\cdot}91\times10^{-4})^2\mathbf{I}_3 & \mathbf{0}_3 & \mathbf{0}_3 \\ \mathbf{0}_3 & \mathbf{0}_3 & (2{\cdot}45\times10^{-4})^2\mathbf{I}_3 & \mathbf{0}_3 \\ \mathbf{0}_3 & \mathbf{0}_3 & \mathbf{0}_3 & (4{\cdot}85\times10^{-7})^2\mathbf{I}_3 \end{pmatrix} \tag{82}$$

The measurement covariance matrix is also considered as follows:

$$\mathbf{R} = \begin{bmatrix} (0{\cdot}1)^2 & 0 & 0 & 0 & 0 & 0 & 0 \\ 0 & (0{\cdot}01)^2 & 0 & 0 & 0 & 0 & 0 \\ 0 & 0 & (0{\cdot}01)^2 & 0 & 0 & 0 & 0 \\ 0 & 0 & 0 & (0{\cdot}01)^2 & 0 & 0 & 0 \\ 0 & 0 & 0 & 0 & (0{\cdot}001)^2 & 0 & 0 \\ 0 & 0 & 0 & 0 & 0 & (0{\cdot}001)^2 & 0 \\ 0 & 0 & 0 & 0 & 0 & 0 & (0{\cdot}1)^2 \end{bmatrix} \tag{83}$$

In Figure 6, the estimated positions in the horizontal (e.g. north and east) direction are shown. Figure 7 also shows the absolute error curves. Absolute error is expressed as the absolute value of the difference between the reference and estimated positions. In

https://doi.org/10.1017/S0373463315000752 Published online by Cambridge University Press

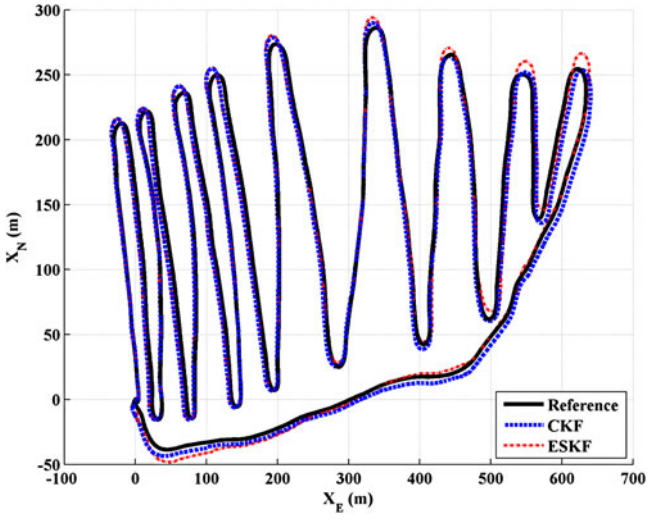

Figure 6. Estimated positions.

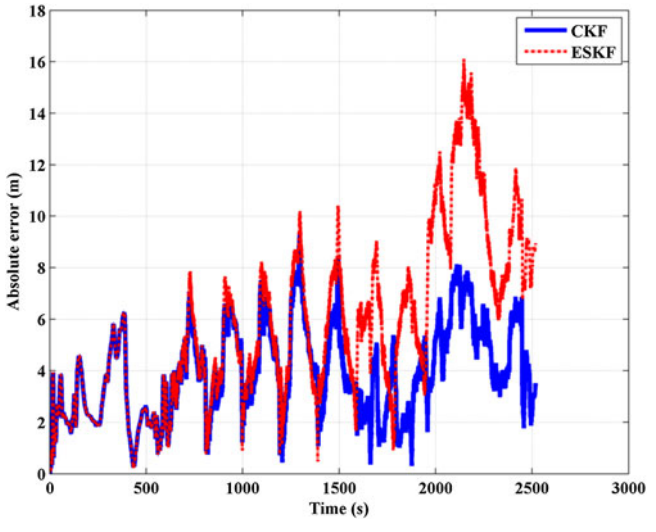

Figure 7. Estimation error.

Figures 8 and 9, the curves of the estimated position absolute errors in the directions of the east and north are depicted, respectively. These curves are defined as the absolute value of the difference between the estimated position in the east (or north) direction and the GPS position in that direction.

Based on these results, the positions estimated by both approaches pursue the reference position with a bounded error. However, due to utilising the more accurate integration method in the proposed navigation system, its estimation error is less than that of the ESKF approach.

https://doi.org/10.1017/S0373463315000752 Published online by Cambridge University Press

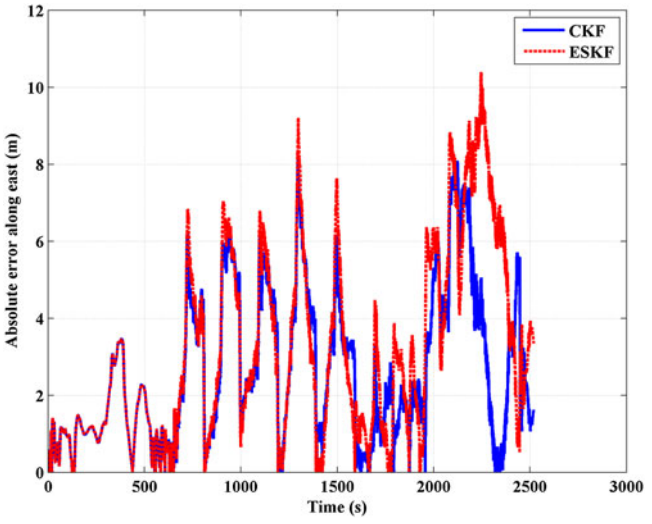

Figure 8. Estimated position errors in the east direction.

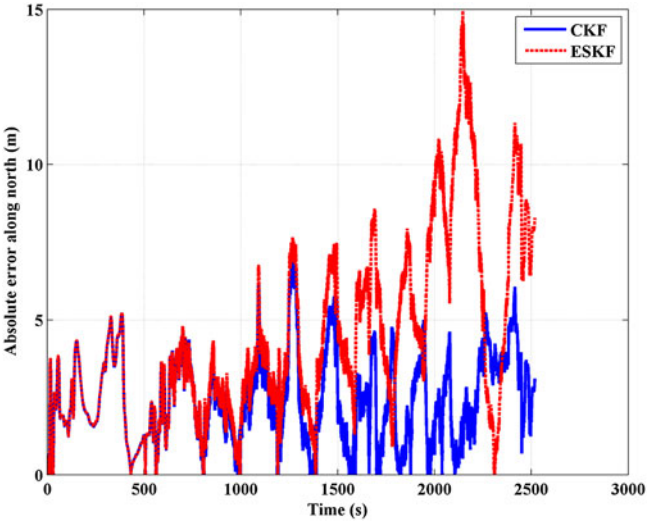

Figure 9. Estimated position errors in the north direction.

In this paper, the Root Mean Square Error (RMSE) and the relative error criteria are used for quantitatively evaluating the performance of the system which is calculated as follows:

$$SE_{\mathrm{k}} = (R_{xk} - E_{xk})^2 + (R_{yk} - E_{yk})^2 + (R_{zk} - E_{zk})^2$$
$$\mathrm{RMSE} = \mathrm{sqrt}[\mathrm{mean}(SE_k)] \tag{84}$$

$$\mathrm{Relative\,RMSE} = \frac{\mathrm{RMSE}}{\mathrm{Travelled\,Distance}} \times 100 \tag{85}$$

https://doi.org/10.1017/S0373463315000752 Published online by Cambridge University Press

Table 2. Performance comparison of the proposed system and conventional ESKF approach.

Approach	RMSE (m)	Relative RMSE (%)	North RMSE/Relative Value (m/%)	East RMSE/Relative Value (m/%)	Max. Position Error (m)
Proposed system	4·3	0·09	2·8/0·067	3·26/0·2	9·3
ESKF	6·5	0·13	5·2/0·12	3·95/0·24	16·1

Where R_i and E_i are the reference and estimated position along the corresponding axis. In this test where the vessel travelled approximately 4897 metres for nearly 42 minutes, the RMSE values of the position estimated by the proposed system and ESKF approach are 4·3 m and 6·5 m and relative errors are 0·09% and 0·13% of the travelled distance, respectively. The maximum position error for the proposed system is 9·3 m, while this value for the ESKF approach is 16·1 m. The RMSE values of the estimated position in the directions of the east and north for the proposed system are 3·26 m and 2·8 m, whereas these values for ESKF approach are 3·95 m and 5·2 m. Therefore, in accordance with the obtained results, the unscented-based integrated navigation system estimates the vehicle position more accurately than the conventional ESKF approach. The results obtained from the practical test for travelled trajectory are summarised in Table 2.

5. CONCLUSIONS. The conventional approach for combining SINS information and the auxiliary data in underwater navigation is the ESKF. In this approach, the errors in the position, velocity and orientation are estimated using the difference between SINS outputs and the auxiliary measurements and the KF operates based on the set of the INS error propagation equations derived from the first order approximation of the Taylor series expansion of the system dynamic and measurement equations. In this paper, in order to reduce the first order linearization effect on the estimation accuracy, an integrated navigation system for underwater applications is designed using unscented filtering. In the proposed system, the total state nonlinear dynamic and measurement models are used and the mean and covariance matrix of the navigation state, whether in the prediction or correction stage, are estimated using the unscented-based integration algorithm. The lake test results show that the proposed approach improves the system performance compared with the conventional ESKF approach.

REFERENCES

Arasaratnam, I. (2009). *Cubature Kalman Filtering: Theory and Applications*. PhD thesis, McMaster University, Hamilton, Ontario, Canada.

Arasaratnam, I. and Haykin, S. (2009). Cubature Kalman Flters. *IEEE Transaction son Automatic Control*, **54**(6), 1254–1269.

Atia, M.M., Karamat, T. and Noureldin, A. (2014). An Enhanced 3D Multi-Sensor Integrated Navigation System for Land-Vehicles. *The Journal of Navigation*, **67**(4), 651–671.

Bar-Shalom, Y., Lee, X.R. and Kirubarajan, T. (2001). *Estimation with Applications to Tracking and Navigation*. John Wiley and Sons, Inc.

https://doi.org/10.1017/S0373463315000752 Published online by Cambridge University Press

Benzerrouk, H., Salhi, H. and Nebylov, A. (2013). Adaptive Cubature and Sigma Points Kalman Filtering Applied to MEMS IMU/GNSS Data Fusion during Measurement Outlier. *Journal of Sensor Technology*, **3**(4), 115–125.

Britting, K.R. (1971). *Inertial Navigation Systems Analysis*. John Wiley and Sons, Inc.

Brokloff, N. (1997). Dead Reckoning with an ADCP and Current Extrapolation.*OCEANS '97. MTS/IEEE Conference Proceedings*, Halifax, NS,6–9 October, 994–1000.

Brown, R.G. and Hwang, P.Y.C. (1997). *Introduction to Random Signals and Applied Kalman Filtering*. John Wiley and Sons, Inc.

Farrell, J.A. (2008). *Aided Navigation GPS with High Rate Sensors*. McGraw-Hill Professional.

Farrell, J.A. and Barth, M. (1999). *The Global Positioning System and Inertial Navigation*. McGraw-Hill Professional.

Foss, H.T. and Meland, E.T. (2007). *Sensor Integration for Nonlinear Navigation System in Underwater Vehicles*. MSc Thesis, Norwegian University of Science and Technology, Trondheim, Norway.

Gao, W., Zhang, Y. and Wang, J. (2014). A Strapdown Interial Navigation System/Beidou/Doppler Velocity Log Integrated Navigation Algorithm Based on a Cubature Kalman Flter. *Sensors*, **14**(1), 1511–1527.

Georgy, J., Karamat, T., Iqbal, U. and Noureldin, A. (2011). Enhanced MEMS-IMU/Odometer/GPS Integration using Mixture Particle Filter. *GPS Solution*, **15**(3), 239–252.

Gilcoto, M., Jones, E. and Farina-Busto, L. (2009). Robust Estimations of Current Velocities with Four-Beam Broadband ADCPs. *Journal of Atmospheric and Oceanic Technology*, **26**(12), 2642–2654.

Grenon, G., An, P.E., Smith, S.M. and Healey, A.J. (2001). Enhancement of the Inertial Navigation System for the Morpheus Autonomous Underwater Vehicles. *IEEE Journalof Oceanic Engineering*, **26**(4), 548–560.

Grewal, M.S. and Andrews, A.P. (2008). *Kalman Filtering Theory and Practice Using MATLAB*. John Wiley and Sons, Inc.

Grewal, M.S., Weill, L.R. and Andrews, A.P. (2007). *Global Positioning System, Inertial Navigation, and Integration*. John Wiley and Sons, Inc.

Groves, P.D. (2008). *Principles of GNSS, Inertial, and Multi-sensor Integrated Navigation Systems*. Artech House.

Hegrenaes, O. and Hallingstad, O. (2011). Model-aided INS with Sea Current Estimation for Robust Underwater Navigation. *IEEE Journalof Oceanic Engineering*, **36**(2), 316–337.

Hide, C., Moore, T., Hill, C. and Park, D. (2006). Low Cost, High Accuracy Positioning In Urban Environments. *The Journal of Navigation*, **59**(3), 365–379.

Jalving, B., Gade, K. and Hagen, O.K. (2003). A Toolbox of Aiding Techniques for the Hugin AUV Integrated Inertial Navigation System. *Oceans 2003 MTS/IEEE*, San Diego, CA, 22–26 September, 1146–1153.

Jekeli, C. (2001). *Inertial Navigation Systems with Geodetic Applications*. Walter de Gruyter GmbH Co.

Jo, G. and Choi, H.S. (2006). Velocity-aided Underwater Navigation System using Receding Horizon Kalman filter. *IEEE Journal of Oceanic Engineering*, **31**(3), 565–573.

Julier, S.J. and Uhmann, J.K. (1997). A New Extension of the Kalman Filter to Nonlinear Systems. *AeroSense'97*, 182–193.

Julier, S., Uhmann, J. and Durrant-Whyte, H.F. (2000). A New Method for the Nonlinear Transformation of Means and Covariances in Filters and Estimators. *IEEE Transactions on Automatic Control*, **45**(3), 477–482.

Julier, S.J. and Uhmann, J.K. (2004). Unscented Filtering and Nonlinear Estimation. *Proceedings of the IEEE*, **92**(3), 401–422.

Kinsey, J.C., Eustice, R.M. and Whitcomb, L.L. (2006). A survey of Underwater Vehicle Navigation: Recent Advances and New Challenges. *IFAC Conference Manoeuvre Control Marine Craft*, Lisbon, Portugal.

Kinsey, J.C. and Whitcomb, L.L. (2007). In Situ Alignment Calibration of Attitude and Doppler Sensors for Precision Underwater Vehicle Navigation: Theory and Experiment. *IEEE Journal of Oceanic Engineering*, **32**(2), 286–299.

Kussat, N.H., Chadwell, C.D. and Zimmerman, R. (2005). Absolute Positioning of an Autonomous Underwater Vehicle using GPS and Acoustic Measurements. *IEEE Journal of Oceanic Engineering*, **30** (1), 153–164.

Larsen, M.B. (2000). Synthetic Long Baseline Navigation of Underwater Vehicles. *OCEANS 2000 MTS/ IEEE Conference and Exhibition*, Providence, RI, 11–14 September, 2043–2050.

Lee, P.M., Jun, B.H., Kim, K., Lee, J., Aoki, T. and Hyakudome, T. (2007). Simulation of an Inertial Acoustic Navigation System with Range Aiding for an Autonomous Underwater Vehicle. *IEEE Journal of Oceanic Engineering*, **32**(2), 327–345.

Leonard, J.J., Bennett, A.A., Smith, C.M. and Feder, H.J.S. (1998). Autonomous Underwater Vehicle Navigation. *Technical Report MIT Marine Robotics Laboratory Technical Memorandum* 98–1, Cambridge, MA.

Marco, D.B. and Healey, A.J. (2001). Command, Control, and Navigation Experimental Results with the NPS ARIES AUV. *IEEE Journal of Oceanic Engineering*, **26**(4), 466–476.

Maybeck, P.S. (1979). *Stochastic Models, Estimation, and Control*. Academic Press.

McEwen, R., Thomas, H., Weber, D. and Psota, F. (2005). Performance of an AUV Navigation System at Arctic Latitudes. *IEEE Journal of Oceanic Engineering*, **30**(2), 443–454.

Miller, P.A., Farrell, J.A., Zhao, Y. and Djapic, V. (2010). Autonomous Underwater Vehicle Navigation. *IEEE Journal of Oceanic Engineering*, **35**(3), 663–678.

Moore, T., Hill, C., Norris, A., Hide, C., Park, D. and Ward, N. (2008). The Potential Impact of GNSS/INS Integration on Maritime Navigation. *The Journal of Navigation*, **61**(2), 221–237.

Niu, X., Nasser, S., Goodall, C. and El-Sheimy, N. (2007). A Universal Approach for Processing any MEMS Inertial Sensor Configuration for Land-Vehicle Navigation. *The Journal of Navigation*, **60**(2), 233–245.

Novatel. (2010). *OEMV Family Installation and Operation User Manual*.http://www.novatel.com/assets/Documents/Manuals/om-20000093.pdf. Accessed 1 April 2015.

Paull, L., Saeedi, S., Seto, M. and Li, H. (2014). AUV Navigation and Localization: A review. *IEEE Journal of Oceanic Engineering*, **39**(1), 131–149.

Pitman, G.R. (1962). *Inertial Guidance*. John Wiley and Sons, Inc.

Sarkka, S. (2013). *Bayesian Filtering and Smoothing*. Cambridge University Press, UK.

Shabani, M., Gholami, A., Davari, N., Emami, M. (2013). Implementation and Performance Comparison of Indirect Kalman Filtering Approaches for AUV Integrated Navigation System using Low Cost IMU. *ICEE2013*, Mashhad, Iran, 1–6.

Shabani, M., Gholami, A., Davari, N. (2015). Asynchronous Direct Kalman Filtering Approach for Underwater Integrated Navigation System. *Nonlinear Dynamics*, **80**(1–2), 71–85.

Simon, D. (2006). *Optimal State Estimation Kalman, H_∞ and Nonlinear Approaches*. John Wiley and Sons, Inc.

Skog, I. and Handel, P. (2009). In-car Positioning and Navigation Technologies a Survey. *IEEE Transaction on Intelligent Transportation Systems*, **10**(1), 4–21.

Stutters, L., Liu, H., Tiltman, C. and Brown, D.J. (2008). Navigation Technologies for Autonomous Underwater Vehicles. *IEEE Transaction on System, Man, Cybernetics*, **38**(4), 581–589.

Titterton, D.H. and Weston, J.L. (2004). *Strapdown Inertial Navigation Technology*. The Institution of Electrical Engineers.

Van der Merwe, R. (2004). *Sigma-Point Kalman Filters for Probabilistic Inference in Dynamic State-Space Models*. PhD thesis, Oregon Health and Science University, USA.

Wan, E.A., Van Der Merwe, R. (2000). The unscented Kalman filter for nonlinear estimation. *Adaptive Systems for Signal Processing, Communications, and Control Symposium* 2000. *AS-SPCC. The IEEE 2000*, Lake Louise, Alta, 153–158.

Yoon, B.D., Yoon, H.N., Choi, S.H., Lee, J.M. (2013). UKF Applied for Position Estimation of Underwater-Beacon Precision. *Proceedings of the 12th International Conference IAS-12*, Jeju Island, Korea, 501–508

Yun, X., Bachmann, E.R., McGhee, R.B. and Whalen, R.H. (1999). Testing and Evaluation of an Integrated GPS/INS System for Small AUV Navigation. *IEEE Journal of Oceanic Engineering*, **24**(3), 396–404.

Zhao, L. and Gao, W. (2004). The Experimental Study on GPS/INS/DVL Integration for AUV. *Proceeding of Position Location Navigation Symposium, PLANS 2004*, 337–340.